Title

The *Klebsiella pneumoniae ter* operon enhances stress tolerance

Authors

Sophia Mason[1a], Jay Vornhagen[1,2a], Sara N. Smith[2], Laura A. Mike[3], Harry L.T. Mobley[2], and Michael A. Bachman[1,2]*

Affiliations

[1]Department of Pathology, Michigan Medicine, University of Michigan, Ann Arbor, United States of America

[2]Department of Microbiology & Immunology, Michigan Medicine, University of Michigan, Ann Arbor, United States of America

[3]Department of Medical Microbiology & Immunology, University of Toledo, Toledo, United States of America

[a]These authors contributed equally to this work

*Corresponding author. Email: mikebach@med.umich.edu

Abstract

Healthcare-acquired infections are a leading cause of disease in patients that are hospitalized or in long-term care facilities. *Klebsiella pneumoniae* (Kp) is a leading cause of bacteremia, pneumonia, and urinary tract infections in these settings. Previous studies have established that the *ter* operon, a genetic locus that confers tellurite oxide (K_2TeO_3) resistance, is associated with infection in colonized patients. Rather than enhancing fitness during infection, the *ter* operon increases Kp fitness during gut colonization; however, the biologically relevant function of this operon is unknown. First, using a murine model of urinary tract infection, we demonstrate a novel role for the *ter* operon protein TerC as a bladder fitness factor. To further characterize TerC, we explored a variety of functions, including resistance to metal-induced stress, resistance to ROS-induced stress, and growth on specific sugars, all of which were independent of TerC. Then, using well-defined experimental guidelines, we determined that TerC is necessary for tolerance to ofloxacin, polymyxin B, and cetylpyridinium chloride. We used an ordered transposon library constructed in a Kp strain lacking the *ter* operon to identify genes required to resist K_2TeO_3- and polymyxin B-induced stress, which suggested that K_2TeO_3-induced stress is experienced at the bacterial cell envelope. Finally, we confirmed that K_2TeO_3 disrupts the Kp cell envelope, though these effects are independent of *ter*. Collectively, the results from these studies indicate a novel role for the *ter* operon as stress tolerance factor, therefore explaining its role in enhancing fitness in the gut and bladder.

Introduction

Klebsiella pneumoniae (Kp) is a pathogenic member of the *Enterobacteriaceae* family (Order *Enterobacterales*) and a cause of pneumonia, UTI, and bloodstream infections (1). Importantly, Kp has a high potential for antibiotic resistance and is the third leading cause of global deaths attributable to pathogens with the potential for antibiotic resistance (2). Infection with antibiotic-resistant Kp is associated with high mortality rates, with mortality rates ranging from approximately 20-40% (3-5). Multiple studies have demonstrated a strong association (odds ratio ~4.0) between gut colonization and infection, indicating that infectious Kp originates from the gut of colonized patients (6-9). Colonization rates are variable, ranging as high as >75% in hospitalized patients (10), though several large studies indicate a colonization rate closer to 20% (6-8), depending on seasonal effects (11). Therefore, Kp can successfully and silently tolerate the hostile gut environment before causing disease (12). More information about the factors that influence Kp colonization and infection is necessary given the high risk of infection posed to patients colonized by Kp, especially in the context of increasing levels of antibiotic resistance.

Our recent work revealed that the presence of the Kp *ter* operon is associated with bacteremia and pneumonia in colonized patients (13). Experimental interrogation of the *ter* operon using an isogenic mutant revealed that the *ter* operon increases Kp fitness during gut colonization rather than conferring a fitness advantage during bacteremia and pneumonia (13, 14). In particular, a *terC* mutant is less fit in mice with an increased abundance of bacteria known to produce short-chain fatty acids (SCFA). SCFAs, specifically acetate, can inhibit the growth of Kp in a pH-dependent manner (15). However, exogenous administration of SCFAs to mice during gut colonization, but not *in vitro*, results in a fitness defect dependent on the *ter* operon. Therefore, the inhibitory effect of SCFAs is dependent on the presence of

specific indigenous gut microbiota (14). This suggests an alternative biological role for the *ter* operon during Kp pathogenesis, wherein this operon is responsive to a yet-undefined stresses.

The molecular function of the *ter* operon is cryptic. This operon confers resistance to the oxyanion form of the rare non-essential trace element tellurium, tellurite oxide (TeO_3^{-2}). Additionally, the mechanism by which TeO_3^{-2} damages bacterial cells is unclear. Tellurium is occasionally grouped with other transition metals, which exhibit antibacterial properties; however, as a chalcogen, its toxicity likely differs from that of transition metals. Furthermore, TeO_3^{-2} is largely absent in the human body or medical settings (16, 17). Therefore, physiologically relevant stress or stresses other than TeO_3^{-2} must explain the strong association between the *ter* operon and Kp pathogenesis. The biochemical mechanisms of TeO_3^{-2}-induced stress affect several critical pathways and therefore induces pleiotropic stress (reviewed in (18)), making it challenging to infer what physiologically relevant stresses interact with the *ter* operon. Thought to be primarily responsible for its toxicity, the strong oxidizing ability of TeO_3^{-2} has several secondary adverse consequences for the bacterial cell (19). The reduction of TeO_3^{-2} creates hydroxyl radicals by inhibiting heme biosynthesis (20). As a result, these hydroxyl radicals abrogate DNA synthesis and protein synthesis, exhaust cellular reductases, and oxidize membrane lipids (21-24). In conjunction with the proposed biochemical mechanism of TeO_3^{-2}-induced stress, the *ter* operon may play a role in resistance to colicins (family A, B, and K) and bacteriophage (16). Notably, many of the biochemical mechanisms of TeO_3^{-2}-induced stress are akin to those that Kp may encounter during its pathogenesis. For example, in the gut where the *ter* operon is conditionally required for complete fitness, colicins are important weapons of bacterial warfare, and host antimicrobial peptides limit pathogen proliferation (25, 26). These stresses kill by attacking the bacterial membrane and DNA similar to the effects of TeO_3^{-2} (25, 26). Therefore, exploring the molecular function of the *ter* operon is likely to reveal interesting facets of Kp pathogenesis.

Here, we interrogate the physiologically relevant role of the Kp *ter* operon and associated TeO_3^{-2}-induced stress. First, we identified a novel role for the *ter* operon as a fitness factor during urinary tract infection (UTI). Concordant with a fitness impact in multiple body sites, we found that the *ter* operon is involved in stress tolerance, a phenotype wherein more tolerogenic cells die slower than less tolerogenic cells in the presence of harmful agents. This phenotype comports with a general, rather than a specific, stress response. Finally, using a systematic approach, we identified novel genes associated with TeO_3^{-2} resistance in Kp lacking the *ter* operon and indeed found that TeO_3^{-2} acts on diverse biological pathways, which corresponds to a need for a general mechanism of stress response. Collectively, these data suggest a role for the *ter* operon in responding to envelope destabilization, resulting in enhanced stress tolerance and potentially explaining how *ter* operon function enhances fitness during UTI and gut colonization.

Results

TerC is a bladder fitness factor during urinary tract infection.

Our previous study in which we identified the strong association between the *ter* operon and infection was limited to patients that developed pneumonia and bacteremia (13). However, Kp is also an important cause of UTI in colonized patients (7, 11). In a previous survey of 2,549 urine associated Kp isolates, we found that 8.4% contained *ter* (14). To test the role of the *ter* operon in UTI, we competed our *terC* mutant and wildtype (NTUH-K2044) strains 1:1 in a well-established murine transurethral infection model (27). Deletion of *terC* is sufficient to confer susceptibility to K_2TeO_3 and is complemented by *terZ-F* (13, 14). Here, we observed a 2-log fitness defect for the *terC* mutant strain in the bladder of infected mice (Fig. 1). Furthermore, the *terC* mutant strain was mostly absent from the bladder of infected mice (only 2/17 with detectable CFU). The observed bladder fitness defect was not due to differences in growth in urine (Fig. S1A-C) and was not observed *ex vivo* in bladder homogenate (Fig. S1D), indicating that the whole organism, or at least viable tissue is required to observe a TerC-dependent fitness defect. The finding that the *ter* operon was required for complete fitness in the bladder *in vivo* was somewhat surprising, as we have previously demonstrated that TerC is required for complete fitness in the gut in a microbiome-dependent manner (14) and bladder-indigenous microbiota are either sparse or absent (28). Therefore, these findings suggest a function for the *ter* operon that explains a role for fitness in both the gut and bladder.

TerC is not required for growth on common sugars.

Given the finding that TerC is necessary for complete fitness in two dissimilar body sites, we turned to a hypothesis-driven approach to identify the mechanisms that unify these phenotypes. Structure-based prediction of the function suggested that TerC may act as a sugar transporter (14). Specifically, the highest-confidence functional predictions were

hexose:proton symporter activity, galactose transmembrane transporter activity, arabinose transmembrane transporter activity, and fucose transmembrane transporter activity. This activity could explain the fitness defect observed in multiple, unrelated body sites, as perturbations in metabolic flexibility are known to impact Kp site-specific fitness, including the gut (29). To test this hypothesis, we compared growth of WT and *terC* mutant strains containing an empty pACYC184 vector (NTUH-K2044 pVector and NTUH-K2044Δ*terC* pVector, respectively) and a *terC* complement strain expressing *terZ-F in trans* (NTUH-K2044Δ*terC* pTerZ-F) in M9 minimal medium supplemented with various sugars at a final concentration of 0.5%. We previously demonstrated that expression of *terZ-F* is required to complement the K_2TeO_3 resistance phenotype (14). TerC was dispensable for growth in the presence of all sugars tested (Figure S2), which include: the hexoses fucose, galactose, glucose, and rhamnose; the pentoses arabinose and xylose; and the disaccharides lactose and sucrose. The NTUH-K2044ΔterC pTerZ-F strain had small but significant growth defects in lactose, sucrose, and rhamnose, and grew significantly better than NTUH-K2044 pVector in galactose based on area under the curve analysis (Figure S2). Although not exhaustive, these data indicate that TerC is not required for growth on these eight common sugars.

TerC is dispensable for resistance to metal and radical oxygen species-induced stress.

We next hypothesized that the *ter* operon may be involved in resistance to transition metal-induced stress. Metal-responsive genes are important fitness factors during UTI (30, 31) and gut colonization (32). Moreover, several transition metal resistance operons are co-localized on *ter* operon containing plasmids (14), suggesting a conserved role for transition metal resistance for these plasmids. To test this hypothesis, we determined the minimum inhibitory concentration (MIC) of several first-row transition metals with known function as

151 micronutrients and that are toxic in excess through induction of redox stress (reviewed in (33)
152 and (34)). As expected, the *terC* mutant strain was more susceptible to K_2TeO_3 than the WT
153 strain, and this phenotype was complemented by expressing *terZ-F in trans* (Figure S3A). No
154 differences in MIC were observed for any transition metals, indicating that the *ter* operon is
155 dispensable for resistance to transition metal-induced stress (Figure S3A). Moreover, the MIC
156 of K_2TeO_3 was substantially lower than that of the tested first-row transition metals, indicating
157 that the biological activity of the first-row transition metals differs from that of K_2TeO_3.

158 As K_2TeO_3 is a potent generator of radical oxygen species (ROS), next we explored the
159 hypothesis that the *ter* operon may be involved in resistance to ROS-induced stress (18, 20).
160 Like metal-induced stress, resistance to ROS has been implicated in bacterial fitness during
161 UTI (35, 36) and gut colonization (37). Moreover, some studies have suggested that the *ter*
162 operon is under transcriptional control by OxyR (38, 39). To test this hypothesis, we
163 determined the impact of TerC on the MIC of three cell-permeable ROS generators: hydrogen
164 peroxide (H_2O_2), and the superoxide-generating redox-cycling compounds paraquat and
165 menadione. As above, TerC was necessary for K_2TeO_3 resistance; however, TerC was
166 dispensable for resistance to H_2O_2, paraquat, and menadione (Figure S3B). Collectively, these
167 data suggest an alternative function for the *ter* operon.
168
169 **TerC plays a role in stress tolerance.**
170 It is perhaps not surprising that the *ter* operon is dispensable for metal and ROS-
171 induced stress, as there are several factors, such as superoxide dismutase, glutathione, and
172 catalase (reviewed in (40)), that play an important role in detoxifying ROS. Correspondingly,
173 metal and ROS resistance genes are important fitness factors during Kp lung infection (41, 42)
174 where the *ter* operon is dispensable (13). It may be the case that the *ter* operon plays a
175 different role in resisting TeO_3^{-2} and the pleiotropic stress it induces. Therefore, we further

considered the structure-function relationship of TerC. While TerC does not appear to be a dedicated sugar transporter, it has been suggested that Ter proteins form a stress-sensing membrane complex anchored by TerC (43). A potential role for TerC in sensing or responding to envelope stress was intriguing, as maintenance of the cell envelope is critical for stress tolerance (44, 45). Notably, TerC is membrane-bound (46).

To explore a role for TerC and the *ter* operon in stress tolerance, we turned to the definitions and guidelines for research on antibiotic persistence (47). These guidelines outline the experimental approach for differentiating stress resistance, tolerance, and persistence. Briefly, resistance is defined as difference in the MIC of a stress, whereas tolerance and persistence are defined as enhanced survival during stress exposure with no change in MIC. Rather, tolerant cells die more slowly during stress exposure, and persister cells are a small subpopulation of tolerant cells that survive stress exposure better than the general population. Mechanistically, tolerance is often mediated by specific, population-wide stress responses (reviewed in (48)), whereas persister cells are a stochastically formed sub-population (reviewed in (49)). These phenotypes can be differentiated by measuring the kill curve in the presence of stress and summarized as the minimum duration of killing at a pre-defined percentage of the initial population ($MDK_{\%}$). Chemical concentrations well above (≥10X MIC) are used for these experiments. Differences in stress tolerance between two populations are defined by differential killing of a large fraction of the initial population, such as differences in 90% (MDK_{90}) or 99% (MDK_{99}). The difference in persistence between two populations is defined by a biphasic kill curve, wherein initial killing occurs as a similar rate (*e.g.*, identical MDK_{90} or MDK_{99}), then transitions to a differential biphasic state, such as differences in 99.9% ($MDK_{99.9}$) or 99.99% ($MDK_{99.99}$) of the initial population.

Using these guidelines, we assessed the role of TerC in stress tolerance. First, we characterized the dynamics of K_2TeO_3-mediated killing and observed more rapid killing of the

terC mutant compared to its parent strain (Figure 2Ai-ii), which was determined to be significantly different based on AUC analysis (Figure 2Aiii) and interpolation of exact MDK values (Figure 2Aiv). Finally, TerC-dependent survival at 4 hours post stress exposure was complemented *in trans* (Figure 2Av). Next, we explored killing dynamics in response to ofloxacin-induced stress. Fluoroquinolones, such as ofloxacin, kill bacterial cells through inhibition of DNA gyrase and are commonly used to generate persister cells in a laboratory setting (50). The MIC of ofloxacin was identical between *terC* mutant and its parent strain (Figure 2Bi), indicating TerC is not an ofloxacin resistance factor. Interestingly, we observed significant differences in the kill curves between these two strains (Figure 2Bii-iii). Interpolation of MDK values revealed a significant difference between the MDK_{90} and MDK_{99} of the *terC* mutant and its parent (Figure 2Biv), indicating that the wildtype strain was significantly more tolerant to ofloxacin-induced stress than the *terC* mutant. The $MDK_{99.9}$ and $MDK_{99.99}$ were incalculable for the wildtype strain, as ofloxacin failed to kill this proportion of cells. As above, TerC-dependent survival at 4 hours post stress exposure was complemented *in trans* (Figure 2Bv). Collectively, these data suggest that TerC may be necessary for ofloxacin tolerance.

To investigate this tolerance phenotype further, we tested a second antibiotic, polymyxin B (PmB), which has a different mechanism of action than ofloxacin: disruption of the bacterial cell envelope. As was observed with ofloxacin, the MIC of PmB was identical for the *terC* and its parent strain (Figure 2Ci). Notably, we observed significant differences in the kill curves between these two strains in response to PmB-induced stress, wherein the wildtype strain was killed more slowly that the *terC* mutant (Figure 2Cii-iii). The MDK_{90} of the *terC* mutant trended lower than its parent strain and the MDK_{99} and $MDK_{99.9}$ was incalculable for the wildtype strain (Figure 2Civ). Complementation *in trans* restored survival at 4 hours post stress exposure (Figure 2Cv). As with ofloxacin, these data indicate that the *terC* mutant is less tolerant to PmB-induced stress than its parent strain. Finally, we repeated these experiments with

cetylpyridinium chloride (CPC), a quaternary ammonium compound that disrupts the cell envelope, leading to leakage of intracellular contents and death (51). As with PmB, no differences between the MIC of the wildtype strain at the *terC* mutant was observed (Figure 2Di); however, the *terC* mutant was killed more rapidly that its parent strain due to CPC-induced stress, which was reflected in all MDK values (Figure 2Dii-iv). Finally, 4-hour post stress exposure survival was complemented *in trans* (Figure 2Dv). Collectively, these data indicate that TerC is necessary for tolerance to stresses with distinct mechanisms of action and potentially explains the requirement of TerC for complete fitness in the gut and bladder.

A systematic screen reveals diverse genes associated with K_2TeO_3 resistance.

The finding that TerC is required for tolerance, but not resistance, to stresses with differing mechanisms of action comports with its requirement for resistance to the pleiotropic stress induced by K_2TeO_3; however, this finding does not implicate a specific pathway or cellular compartment of action for the *ter* operon. To determine if K_2TeO_3 acts on a specific pathway or cellular compartment, we turned to a systematic approach to identify genes and pathways required to mitigate the effects of the K_2TeO_3-induced stress when the *ter* operon was absent. To this end, we employed an ordered, condensed transposon (Tn) library constructed in the Kp strain KPPR1, which doesn't encode the *ter* operon and is susceptible to K_2TeO_3 (Figure 3A-B). This Tn library contains individual insertions in 3,733 genes, covering 72% of all available open reading frames in the genome (52). First, we determined the concentration at which KPPR1 growth was partially inhibited by K_2TeO_3 to be approximately 1 μM. We aimed to screen our Tn library at this concentration to identify mutants conferring both resistance (increase in growth) and susceptibility (decrease in growth) to K_2TeO_3. We then cultured each mutant in the presence of 1 μM K_2TeO_3 and assessed growth by measuring growth at OD_{600} (Figure 3C). If the growth of a mutant was two standard deviations above or

below the mean growth of all mutants, we categorized the interrupted gene as potentially being important for K_2TeO_3 resistance. Initially, we found 129 candidate susceptible mutants and 15 candidate resistant mutants (Figure 3C). It was not surprising that we identified more susceptible than resistant mutants, as previous studies using other bacteria to identify genes involved in K_2TeO_3 resistance required several passages in the presence of K_2TeO_3 to identify such loci (20). As our screen was performed at a standard concentration of K_2TeO_3, we next aimed to validate our candidate mutants. We preliminarily excluded 14 mutants due to an observed growth defect in LB in the absence of K_2TeO_3. We then determined the concentration of K_2TeO_3 that inhibited 50% of bacterial growth (IC_{50}) for our remaining candidates. Of the 138 candidates, 79 had a K_2TeO_3 IC_{50} that corroborated our original screen, and 29 had a significantly lower ($q \leq 0.1$) IC_{50} value than that of the parent strain (Table 1, Figure 3D, Table S1). To further characterize these genes associated with K_2TeO_3 resistance, we assessed the gene function using the Kyoto Encyclopedia of Genes and Genomes (KEGG) (Figure 3E, Table S1). Metabolism (n = 12/29) and “Other” (n = 12/29) were the most well-represented categories. Assignment of more granular function of these genes revealed that the most common function was carbohydrate metabolism (n = 5/29), followed by genetic information processing (n = 4/29). These findings suggest that many diverse genes are necessary for growth in the presence of K_2TeO_3, rather than a set of related genes with conserved function.

To determine if genes involved in K_2TeO_3 resistance are also involved in resistance to stressors where TerC was required for tolerance, we screened mutants validated for increased K_2TeO_3 sensitivity for growth in the presence of PmB. Interestingly most genes involved in K_2TeO_3 resistance were also required for growth in the presence of PmB (Figure 3F). The pyruvate dehydrogenase complex (*aceF*, *aceE*, *pdhR*) was one notable exception to this finding. Given that PmB is a membrane-active antibiotic, this finding further supports the indication that K_2TeO_3 destabilizes the Kp envelope. Moreover, this suggests that the function

of the *ter* operon is to aid in envelope stabilization or respond to envelope destabilization, leading to enhanced stress tolerance, and enhanced fitness in the gut and bladder.

Gene ontology biological process enrichment analysis revealed a single enriched pathway amongst these individual genes: enterobacterial common antigen (ECA) biosynthetic process (42.23-fold enrichment, FDR P value = 5.25×10^{-2}). Notably, additional ECA genes *wecG*, *wecA* narrowly missed our validation criteria (Table S1). This finding supports a potential role for the *ter* operon in maintaining envelope stability or responding to envelope destabilization, which comports with a role in stress tolerance.

K_2TeO_3 disrupts the Kp cell envelope

Given that the finding that many genes associated with K_2TeO_3 resistance in a strain lacking *ter* may play a role in maintaining envelope stability we next aimed to determine if K_2TeO_3 disrupts the cell envelope, and if the *ter* operon stabilizes the envelope. Fluorescence-based Ethidium bromide (EtBr) accumulation assays can be used to assess envelope damage (53, 54), wherein EtBr accumulates in the periplasm or intercalates in cellular DNA following cell envelope disruption. As colistin has been shown to disrupt both the outer and inner membrane of the Gram-negative envelope (55), we used PmB as a positive control. Following exposure to K_2TeO_3 and PmB at the same concentrations used in killing assays (Figure 2), Kp displayed higher levels of EtBr accumulation than that of the no treatment controls (Figure 4). This phenotype was independent of TerC, suggesting that the effects of *ter* are downstream of initial disruption of the cell envelope (Figure 4). These data demonstrate that K_2TeO_3 disrupts the cell envelope and in conjunction with the data in Figure 2Aii (difference in fraction recovered at 60 minutes post-K_2TeO_3 exposure) suggest that the effects of *ter* are downstream of envelope destabilization.

DISCUSSION

The work presented here advances our understanding of the physiological role of the Kp *ter* operon. Our results indicate that a physiological role of the *ter* operon is to respond to envelope stress during colonization and infection of specific body sites to tolerate these stressful environments and enhance fitness. These effects are likely downstream of the initial insult to the envelope. Previously, we have shown that this cryptic operon is highly associated with Kp pneumonia and bacteremia in colonized patients (13), and further work demonstrated that this association was due to a TerC-dependent fitness advantage conferred in the gut (14). Here, we demonstrate a novel role for TerC as a fitness factor during urinary tract infection. The identification of TerC as a bladder fitness factor using a hypervirulent Kp strain (NTUH-K2044) is noteworthy, as several recent reports have indicated that hvKp are an important cause of asymptomatic bacteriuria and UTI (56-60). As hypervirulent strains become more prevalent and hypervirulent, antibiotic resistant strains emerge, it is critical to identify compartment-specific fitness factors (61, 62). Additionally, this finding that TerC is a fitness factor during urinary tract infection implies a conserved mechanism of fitness enhancement in the gut and bladder that is dispensable in the lung and blood (13, 14).

To identify this conserved mechanism, we first focused on known mechanisms of K_2TeO_3-induced stress that functionally overlap gut and bladder fitness factors. We determined that TerC is dispensable for metal and ROS resistance. We also determined that TerC is dispensable for the transport of several common sugars. Rather, we identified a novel role for TerC in stress tolerance, wherein Kp lacking TerC were killed more rapidly in the presence of several stresses. Given the pleiotropic effects of K_2TeO_3 on the bacterial cell, a role for the *ter* operon during general stress response is appealing. This could explain how the *ter* operon enhances fitness in biologically distinct sites, where the specific stresses Kp encounters are likely to differ. To identify a specific function for the *ter* operon, we undertook a systematic

screen of K_2TeO_3 resistance in a Kp strain that lacks the *ter* operon. This screen did not reveal a consensus molecular function or specific cellular compartment of action but did suggest that K_2TeO_3-induced stress is primarily experienced at the cell envelope. Several of these genes were also required for growth in the presence of PmB, which is a membrane-active antibiotic. This finding affirms the necessity for TerC during stress tolerance. Finally, we demonstrate that K_2TeO_3 disrupts the cell envelope, though these effects were independent of *ter*, which suggests an indirect means of responding to envelope stress.

The finding that TerC enhances stress tolerance is an appealing explanation for its role in gut colonization. Host- and microbiota-derived antimicrobial peptides are critical mediators of gut homeostasis and bacterial infection (63-65). Microbiota-synthesized antimicrobial peptides are known as bacteriocins. The ability of colonizing Kp to tolerate antimicrobial peptide- and bacteriocin-mediated stress may be critical to its success in the gut when the indigenous microbiota is intact. Indeed, early experiments interrogating the biological function of the *ter* operon suggested a potential role for resisting pore-forming bacteriocins (16). Moreover, PmB is a cyclic peptide and therefore mimics the mechanism of action of many antimicrobial peptides. The necessity of TerC for tolerance to PmB suggests that TerC may also be required for tolerance to other antimicrobial peptides found in the bladder and/or gut.

Tolerance has received significant attention due to its contribution to antibiotic treatment failure and the development of antibiotic resistance; however, this neglects the role of tolerance to other stress induced by factors not characterized as classical antibiotics, such as bacteriocins or detergents. This is especially relevant in the context of PmB. Polymyxins bind to LPS in the outer and cytoplasmic membrane, resulting in cell lysis and death (55). The finding that TerC is necessary for tolerance to PmB supports the assertion proposed in other studies that the Ter proteins form a stress-sensing membrane complex that may influence transmembrane permeability (43). Similarly, the quaternary ammonium compound CPC kills

bacterial cells through integration into and disruption of the cell envelope. The biological relationship between TerC and ofloxacin tolerance is less clear, though membrane peptide TisB enhances tolerance to ciprofloxacin through disruption of the proton motive force (66). Additionally, several mechanistically divergent antibiotics, including fluoroquinolones, induce inner membrane damage and cytoplasmic condensation, leading to bacterial cell death (67). Therefore, destabilization of the cell envelope may have secondary effects that impact tolerance. Exploration of TerC-dependent tolerance to other diverse stresses is likely to further refine our understanding of the biology of the *ter* operon.

Our systematic screen of K_2TeO_3 resistance revealed both expected and novel loci associated with K_2TeO_3 resistance (Table 1). Interruption of the pyruvate dehydrogenase complex resulting in increased K_2TeO_3 susceptibility was expected and serves as validation of the approach, as the heterologous expression of *aceE and aceF* leads to enhanced K_2TeO_3 resistance (68). Commensurately, TehB is a known K_2TeO_3 resistance protein that, in conjunction with TehA, confers resistance through the volatilization of tellurite through methyltransferase activity (18). An insertion mutant in *tehA* was not present in our Tn library. The finding that the ECA synthesis locus is a significant contributor to K_2TeO_3 resistance is particularly intriguing, as this conserved locus has been implicated in many critical facets of the biology of Enterobacterales. ECA is a carbohydrate structure characteristically found in the bacterial envelope, where it is attached to LPS and peptidoglycan (reviewed in (69)). Disruption in Kp reduces virulence in murine pneumonia and bacteremia models, though this phenotype is largely dependent on the stability of LPS, rather than ECA itself (70). Regardless of whether the observed K_2TeO_3 resistance phenotype is dependent on LPS stability, the envelope appears to be a critical mediator of K_2TeO_3 resistance for Kp independent of *ter*. A role for envelope stability in K_2TeO_3 resistance is also supported by increased K_2TeO_3 sensitivity of the *bamB*, *gmhB*, and *mdoG* mutants. The Bam complex (BamABCDE) is

responsible for the proper insertion of proteins into the outer membrane (reviewed in (71)), GmhB plays a role in LPS biosynthesis (72, 73), and MdoGH is critical for the biosynthesis of osmoregulated periplasmic glucans (reviewed in (74)). Therefore, disruption of these genes or the ECA biosynthesis locus may result in a de-stabilized envelope.

Although this study revealed novel aspects of the biology of the *ter* operon, it is not without its limitations. First, this study provides insight into the function of the *ter* operon, but the molecular mechanisms underlying its function remain unknown. Second, the use of a transposon library that is comprised of single-gene insertions may limit the ability to identify every gene involved in K_2TeO_3 resistance. Some of these insertions may not sufficiently disrupt gene function to the same degree as alternative insertions present in a more complex library. Finally, experiments in this study were limited to two strains: the *ter* operon containing strain NTUH-K2044 and the *ter* operon lacking strain KPPR1. The use of these strains is convenient due to available molecular tools and because they are well-characterized; however, both strains are hypervirulent stains, and therefore do not represent the complete genomic breadth of Kp. While the *ter* operon is highly associated with hypervirulent Kp, it is not limited to hypervirulent strains (14). Interestingly, an analogous study using a murine UTI model reported similar bladder bacterial loads using a non-hypervirulent strain (75). Future studies dissecting the function of the *ter* operon should consider both hypervirulent and non-hypervirulent Kp strains. Despite these limitations, this study represents a significant advancement in our understanding of the role of the *ter* operon during Kp pathogenesis.

MATERIALS AND METHODS

Ethics statement

Human sample collection was approved by and performed in accordance with the Institutional Review Boards (IRB) of the University of Michigan Medical School (Study number HUM00004949). Animal studies were performed in strict accordance with the recommendations in the Guide for the Care and Use of Laboratory Animals [102]. The University of Michigan Institutional Animal Care and Use Committee approved this research (PRO00009173).

Materials, media, and bacterial strains

All materials and chemicals were purchased from Sigma-Aldrich (St. Louis, MO) or Fisher Scientific (Hampton, NH) unless otherwise noted. The construction and validation of the isogenic *terC* mutant, the pTerZ-F complementation plasmid, and empty vector and complemented strain is described elsewhere (13, 14). All strains were grown in the presence of appropriate antibiotics for all experiments.

Murine UTI model

The ascending UTI model used in this study has been described elsewhere (27, 76, 77). Briefly, the NTUH-K2044 and NTUH-K2044Δ*terC* strains were cultured overnight from single colonies in LB at 37° C. After overnight growth, strains were mixed 1:1 and adjusted to a final concentration of 2 x 10^9 CFU/mL in sterile PBS. An aliquot of this inoculum was plated on LB broth containing appropriate antibiotics and plates were incubated overnight 27° C to enumerate input CFU and exact ratio. Then, mice were anesthetized with a weight-appropriate dose (0.1 ml for a mouse weighing 20 g) of ketamine-xylazine (80 to 120 mg/kg ketamine and 5 to 10 mg/kg xylazine) by intraperitoneal injection. 50 µL of inoculum was administered

transurethrally into male CBA/J mice over a 30 second period to deliver 10^8 CFU per mouse. After 48 hours, urine was collected, mice were euthanized by inhalant anesthetic overdose and the bladder was collected in sterile PBS. Bladders were homogenized, and all samples were plated on LB containing appropriate antibiotics using an Autoplate 4000 (Spiral Biotech, Norwood, MA) and incubated overnight 27° C to enumerate CFU. Bladder homogenates for growth assays were prepared from uninfected mice. Bladders were collected into 1 mL sterile PBS, homogenized, then centrifuged at 21,130 x *g* for 5 min at 4°C to pellet contaminating bacteria, then supernatant was stored at -80°C until use.

Human urine collection

Human urine was collected from women (ages 21-40) from whom informed consent had been obtained, who have no symptoms of UTI or bacteriuria, and who had not taken antibiotics in the prior two weeks. De-identified samples from least four volunteers were pooled and filter sterilized using a 0.22-µm filter (MilliporeSigma, Burlington, MA), as previously described (77).

Growth assays

The NTUH-K2044 pVector, NTUH-K2044Δ*terC* pVector, and NTUH-K2044Δ*terC* pTerZ-F strains were cultured overnight from single colonies in M9 minimal medium containing 0.5% glucose (M9-Glu), then diluted to OD_{600} of 0.01 in M9 minimal medium containing 0.4% or 0.5% arabinose, fucose, galactose, glucose, lactose, rhamnose, sucrose, xylose, 100% human urine, or 100% murine bladder homogenate. 100 µL of this subculture was plated into a single well of a U bottom 96-well plate in triplicate, then that plate was sealed using optical adhesive film (Applied Biosystems, Waltham, MA). This plate was incubated at 37° C with aeration and OD_{600} readings were taken every 15 min using an Eon microplate reader with Gen5 software

(Version 2.0, BioTek, Winooski, VT) for 24 hours. Area under the curve was quantified using Prism 8 (GraphPad Software, La Jolla, CA).

Minimum inhibitory concentration determination

The NTUH-K2044, NTUH-K2044Δ*terC*, NTUH-K2044 pVector, NTUH-K2044Δ*terC* pVector, and NTUH-K2044Δ*terC* pTerZ-F strains were cultured overnight from single colonies in M9-Glu. Overnight cultures were diluted to 10^7 CFU/mL into M9-Glu with a 2X concentration of strain-appropriate antibiotics. Then, metals, ROS generators, antibiotics, biocides, or K_2TeO_3 was diluted in M9-Glu to 2X final concentration. 100 µL of this solution was plated into a single well of a U bottom 96-well plate in triplicate, then 2-fold serial diluted into M9-Glu 10 times, discarding 50 µL of the last dilution to achieve a final volume of 50 µL in each well, leaving the last well as only media. Finally, 50 µL of the 2X culture dilution was plated across each serial dilution to achieve a final cell density of 5 x 10^6 CFU/mL. This plate was sealed using optical adhesive film (Applied Biosystems, Waltham, MA) and incubated at 37° C for 24 hours. After 24 hours, the MIC of each compound was defined as the lowest concentration that fully inhibited bacterial growth. Due to the opacity of high concentration metal solutions, MICs of metals were confirmed by replicate plating onto LB-agar and overnight culture at 37° C.

Killing assays

The NTUH-K2044, NTUH-K2044Δ*terC*, NTUH-K2044 pVector, NTUH-K2044Δ*terC* pVector, and NTUH-K2044Δ*terC* pTerZ-F strains were cultured overnight from single colonies in M9-Glu. To ensure culture uniformity, overnight cultures were diluted 1:1,000 into fresh M9-Glu. Following overnight growth, 500 µL of culture was removed, cells were pelleted at 10,000 x *g* for 3 min, washed once in 500 µL sterile phosphate-buffered saline (PBS), then

resuspended in 500 µL sterile PBS and serial plated onto LB-agar containing appropriate antibiotics to determine initial cell density. Then, K_2TeO_3, ofloxacin, polymyxin B, and cetylpyridinium chloride were added to these cultures to a final concentration of 1 mM, 250 µg/mL, 500 µg/mL, and 25 µM, respectively, from stocks prepared in M9-Glu. 500 µL of culture was removed at indicated time points, and cells were processed as above. All plates were incubated overnight at 27° C, and bacterial CFU/mL was quantified after overnight growth. Bacterial killing was summarized as the fraction of bacterial cells recovered at each timepoint, wherein the CFU/mL at a given timepoint was normalized to the initial CFU/mL. Area under the curve was calculated and minimum duration killing was interpolated from kill curves following log transformation of fraction recovered values using Prism 8 (GraphPad Software, La Jolla, CA).

Tn library screen

Construction, ordering, and condensation of the KPPR1 Tn library has been described elsewhere (41, 52). This arrayed library was cultured overnight in flat bottom 96-well plates at 37° C in LB containing 40 µg/mL kanamycin. After overnight growth, arrayed Tn insertion mutants were sub-cultured into U bottom 96-well plates LB containing 40 µg/mL kanamycin and 1 µM K_2TeO_3 and cultured overnight at 37° C. Bacteria growth after 24 hours was measured at OD_{600} using an Eon microplate reader with Gen5 software (Version 2.0, BioTek, Winooski, VT). This assay was independently repeated twice to achieve three replicates of K_2TeO_3 growth. Candidate genes involved in K_2TeO_3 resistance were those where the mean growth in the presence of 1 µM K_2TeO_3 was two standard deviations above (mean OD_{600} = 0.980) or below (mean OD_{600} = 0.495) the mean of growth of all strains (mean OD_{600} = 0.738). Candidate insertion mutants and the parent strain KPPR1 were then cultured

overnight from single colonies in LB containing appropriate antibiotics. Overnight cultures were diluted to 10^7 CFU/mL into LB with a 2X concentration of appropriate antibiotics. Then, K_2TeO_3 was diluted in LB to 2X final concentration. Serial dilution was performed as above (see "Minimum inhibitory concentration determination"), except the 2X K_2TeO_3 solution was serially diluted 6 times instead of 10. 2X culture dilution was then plated across each serial dilution and the plate was sealed using optical adhesive film (Applied Biosystems, Waltham, MA) and incubated at 37° C for 24 hours. Bacterial growth was measured at OD_{600} using an Eon microplate reader with Gen5 software (Version 2.0, BioTek, Winooski, VT) and exact IC_{50} values were interpolated using a sigmoidal four-parameter logistic curve using Prism 8 (GraphPad Software, La Jolla, CA). This was repeated 3-5 times per candidate insertion mutant. Candidate insertion mutants were considered validated if their mean exact IC_{50} value was high or lower than the parent KPPR1 strain corresponding to their original screen results.

To further characterize validated insertion mutations, gene name, annotation, and BRITE Functional Hierarchies were assigned using the Kyoto Encyclopedia of Genes and Genomes (78, 79) using the VK055 gene number as the search criteria. Cellular compartment was assigned using gene ontology terms in UniProt (80). GO enrichment analysis was performed using the PANTHER Overrepresentation Test (release 2021-02-24) *Escherichia coli* as the reference list (81). For validation experiments, insertion mutants and the parent strain KPPR1 were cultured at 37° C in LB broth containing appropriate antibiotics and arrayed into flat bottom 96-well plates in triplicate. Then, arrayed insertion mutants were diluted 1:100 into LB broth containing appropriate antibiotics and 0.5 μg/mL polymyxin B in U bottom 96-well plates. Plates were sealed optical adhesive film (Applied Biosystems, Waltham, MA) and incubated at 27° C for 24 hours. After 24 hours, bacterial growth was measured at OD_{600} using an Eon microplate reader with Gen5 software (Version 2.0, BioTek, Winooski, VT). This assay was repeated twice more to achieve three replicates.

519

520 **Ethidium bromide accumulation assay**

521 The NTUH-K2044 pVector, NTUH-K2044Δ*terC* pVector, and NTUH-K2044Δ*terC* pTerZ-
522 F strains were cultured overnight from single colonies in M9-Glu. Following overnight growth,
523 approximately 2 x 10^9 CFU were harvested by centrifugation, resuspended in 2 mL of sterile
524 PBS with or without 1 mM K_2TeO_3 or 500 µg/mL polymyxin B, and incubated at 37° C with
525 shaking at 225 rpm. 1 mL of cells were immediately removed, harvested by centrifugation,
526 resuspended in 1 mL of PBS containing 10 µM ethidium bromide, and incubated at room
527 temperature in the dark for 10 minutes. Following incubation, fluorescence was measured in
528 black-walled, clear-bottomed 96-well plates using an excitation of 510 nm and emission of 600
529 nm using a Synergy H1 Hybrid Multi-Mode microplate reader with Gen5 software (Version 2.0,
530 BioTek, Winooski, VT). Bacterial density was measured in tandem at OD_{600}. This procedure
531 was repeated after 60 minutes of exposure to PBS with or without K_2TeO_3 or polymyxin B.
532 Fluorescence was normalized to bacterial density, then fold change in relative fluorescent units
533 was determined by dividing normalized relative fluorescent units at 60 minutes to normalized
534 relative fluorescent units at 0 minutes.

535

536 **Statistical analysis**

537 For *in vitro* studies, all experimental replicates represent biological replicates performed
538 on different days. For statistical analysis, experimental values were log transformed and two-
539 tailed ratio paired t test or RM one-way ANOVA followed by Tukey's multiple comparison test
540 was used to determine significant differences between groups. For *in vivo* studies, all
541 experiments were repeated twice with independent bacterial cultures. Following CFU
542 quantification, competitive indices ((CFU mutant output/CFU WT output)/(CFU mutant
543 input/CFU WT input)) were calculated, then log transformed and a one-sample t test compared

544 to a hypothetical value of 0 was used to determine significance. The limit of detection was
545 used for the CFU output value in the case that no mutant or WT CFU were recovered in the
546 experimental output. A P value of less than 0.05 was considered statistically significant for all
547 experiments, and analysis was performed using Prism 8 (GraphPad Software, La Jolla, CA).
548

FIGURE LEGENDS

Figure 1. TerC is necessary for complete fitness in the bladder during urinary tract infection

Mice were transurethrally inoculated with approximately 10^8 CFU of a 1:1 mix of WT NTUH-K2044 and NTUH-K2044Δ*terC*. (A) Bacterial burden in the urine and bladder was measured after 48 hours, and (B) $\log_{10}$ competitive index (CI) of the mutant strain compared to the WT strain was calculated for each organ (N = 17, mean displayed, ****P < 0.00005, one-sample *t*-test). From 20 inoculated mice, CFU were recovered from 17 mice. The numbers above each column in A indicate the number of mice (of 17) with detectable CFU. Blue circles had no recoverable NTUH-K2044Δ*terC*. CI was calculated using the limit of detection CFU value when no CFU were recovered.

Figure 2. TerC is necessary for tolerance to several stresses

The (A) K_2TeO_3 minimum inhibitory concentration (i, n = 5 independent experiments, median displayed, **P < 0.005, ratio paired *t*-test) was calculated for NTUH-K2044 and NTUH-K2044Δ*terC* strains using broth microdilution. Kill curves (ii, n = 7 independent experiments, mean displayed ± SEM) were generated for these strains using by adding a standard K_2TeO_3 concentration of 1 mM to overnight cultures and (iii) AUC and (iv) MDK were calculated from these kill curves (n = 7 per group, *P < 0.05, **P < 0.005, ratio paired *t*-test, ∞ indicates an incalculable MDK). Finally, NTUH-K2044 pVector, NTUH-K2044Δ*terC* pVector, and NTUH-K2044Δ*terC* pTerZ-F survival was assessed at 4 hours (240 minutes) post 1 mM K_2TeO_3 exposure (v, n = 6-7 independent experiments, median displayed, *P < 0.05, **P < 0.005, ***P < 0.0005, one-way ANOVA followed by Tukey's multiple comparison test). These experiments were repeated for ofloxacin (B), polymyxin B (PmB, C), and cetylpyridinium chloride (CPC, D).

The standard concentrations for killing assays for ofloxacin, polymyxin B, and cetylpyridinium chloride were 250 μg/mL, 500 μg/mL, and 25 μM, respectively. For iii, iv, and v, connecting lines indicate paired biological replicates.

Figure 3. Systematic screen of K_2TeO_3 resistance

The KPPR1 strain, which lacks the *ter* operon, and the NTUH-K2044 and NTUH-K2044Δ*terC* strains were cultured in increasing concentrations of K_2TeO_3 (A) and area under the curve (AUC) was calculated from these dose-response curves (B, mean displayed ± SEM, ****P < 0.0005, one-way ANOVA followed by Tukey's multiple comparison test). (C) 3,733 individual Tn insertion mutants were cultured in the presence of 1 μM K_2TeO_3 and measured at OD_{600}. The blue line is the mean OD_{600} and the red lines are ± 2 S.D. from the mean. Each symbol is an individual mutant, ordered by their gene number (VK055_#). (D) Exact K_2TeO_3 IC_{50} values of validated Tn insertion mutants (n = 3-5 independent experiments). (E) KEGG BRITE Functional Hierarchies were assigned for validated Tn insertion mutants. The highest order hierarchies are shown in the horizontal stacked bar chart, and the second highest order hierarchies are shown in the unstacked bar chart. (F) Validated Tn insertion mutants were cultured in the presence 0.5 μg/mL PmB (n = 3 independent experiments).

Figure 4. EtBr accumulates in K_2TeO_3 and polymyxin B treated Kp.

Stationary phase NTUH-K2044 pVector, NTUH-K2044ΔterC pVector, and NTUH-K2044ΔterC pTerZ-F were exposed to 1 mM K_2TeO_3 or 500 μg/mL PmB. EtBr accumulation (fluorescence) was measured at baseline and at one-hour post-exposure (n = 6 independent experiments, mean displayed, *P < 0.05, **P < 0.005, ***P < 0.0005, one-way ANOVA followed by Tukey's multiple comparison test).

TABLES

Table 1. Insertion mutants involved in K_2TeO_3 resistance

Gene Name	Annotation	Subcellular Location	K2TeO3 IC50±SEM (KPPR1 = 1.11±0.09)	P Value	q Value
VK055_0140_fadR	fatty acid metabolism transcriptional regulator FadR	cytoplasm	0.37±0.06	0.003060	0.010447
VK055_0310	bacterial regulatory helix-turn-helix, lysR family protein		0.29±0.11	0.000093	0.000656
VK055_0397_ccmE	cytochrome c-type biogenesis protein CcmE	integral component of membrane	0.44±0.17	0.002301	0.009113
VK055_0538_tehB2	tellurite resistance protein TehB	cytoplasm	0.47±0.08	0.006082	0.019425
VK055_0986	hypothetical protein	N/A	0.35±0.08	0.001477	0.006521
VK055_1353	putative L,D-transpeptidase YcfS	periplasmic space	0.50±0.11	0.027590	0.068284
VK055_1404	periplasmic glucans biosynthesis protein MdoG	periplasmic space	0.36±0.11	0.001024	0.005068
VK055_1833_nagA	N-acetylglucosamine-6-phosphate deacetylase NagA	cytoplasm	0.40±0.16	0.002208	0.009106
VK055_1870_lipB	lipoyl(octanoyl) transferase LipB	cytoplasm	0.38±0.09	0.002789	0.009860
VK055_2134	putative dTDP-glucose pyrophosphorylase		0.21±0.02	0.000011	0.000120
VK055_2352_yaeD	D,D-heptose 1,7-bisphosphate phosphatase GmhB	cytoplasm	0.26±0.10	0.000020	0.000176
VK055_2373_lpxD	UDP-3-O-[3-hydroxymyristoyl] glucosamine N-acyltransferase LpxD	cytoplasm	0.37±0.08	0.002434	0.009268
VK055_2402_mrcB	penicillin-binding protein 1B MrcB	peptidoglycan-based cell wall	0.38±0.09	0.002789	0.009860
VK055_2451_aceF	pyruvate dehydrogenase E2 component AceF	cytoplasm	0.01±0.00	0.000001	0.000001
VK055_2452_aceE	pyruvate dehydrogenase E1 component AceE		0.29±0.27	0.000001	0.000001
VK055_2453_pdhR	transcriptional repressor for pyruvate dehydrogenase complex PdhR	cytoplasm	0.03±0.01	0.000001	0.000001
VK055_2524_surA	peptidyl-prolyl cis-trans isomerase SurA	periplasmic space	0.08±0.05	0.000001	0.000001
VK055_2525_pdxA2	4-hydroxythreonine-4-phosphate dehydrogenase PdxA2	cytoplasm	0.02±0.00	0.000001	0.000001
VK055_2558_nhaA	na+/H+ antiporter NhaA	integral component of membrane	0.45±0.06	0.015340	0.039965
VK055_2895_miaA	tRNA dimethylallyltransferase MiaA	cytoplasm	0.49±0.16	0.013757	0.038914
VK055_3142_tatC	sec-independent protein translocase protein TatC	integral component of membrane	0.45±0.07	0.014802	0.039606
VK055_3167_dapF	diaminopimelate epimerase DapF	cytoplasm	0.29±0.08	0.000148	0.000977

VK055_3181	enterobacterial common antigen polymerase WzyE	integral component of membrane	0.14±0.00	0.000001	0.000002
VK055_3182_wecF	dTDP-N-acetylfucosamine:lipid II N-acetylfucosaminyltransferase WecF	integral component of membrane	0.34±0.07	0.001236	0.005826
VK055_3188	UDP-N-acetyl-D-mannosaminuronic acid dehydrogenase WecC		0.36±0.17	0.000323	0.001880
VK055_3709	shikimate kinase AroK	cytoplasm	0.33±0.06	0.000970	0.005055
VK055_3906	hypothetical protein	N/A	0.23±0.04	0.000021	0.000177
VK055_4658_yfgL	outer membrane protein assembly factor BamB	integral component of membrane	0.21±0.04	0.000007	0.000088
VK055_5053	DNA gyrase inhibitor SbmC	cytoplasm	0.43±0.11	0.008174	0.025287

599

Acknowledgements

The authors would like to thank the members of the Mobley and Bachman labs for their thoughtful feedback on this study. The authors would also like to thank the urine donors for their contribution to this study.

Funding

This work was supported by funding from National Institution of Health (https://www.nih.gov/) grants 1K99 AI153483-02 to JCV, R01 AI125307 to MAB, and K22 A1145849 to LAM. The funders had no role in study design, data collection and analysis, decision to publish, or preparation of the manuscript.

Author contributions

Conceptualization: SM, JV, MAB

Methodology: JV, LAM, HLTM, MAB

Investigation: SM, JV, SNS

Visualization: JV

Funding acquisition: JV, HLTM, MAB

Project administration: MAB

Supervision: HLTM, MAB

Writing – original draft: SM, JV, MAB

Writing – review & editing: SM, JV, SNS, LAM, HLTM, MAB

Competing interests

Authors declare that they have no competing interests.

Data and materials availability

All source data for this study are provided with this manuscript.

REFERENCES

1. Magill SS, Edwards JR, Bamberg W, Beldavs ZG, Dumyati G, Kainer MA, Lynfield R, Maloney M, McAllister-Hollod L, Nadle J, Ray SM, Thompson DL, Wilson LE, Fridkin SK. 2014. Multistate Point-Prevalence Survey of Health Care–Associated Infections. New England Journal of Medicine 370:1198-1208.

2. Antimicrobial Resistance C. 2022. Global burden of bacterial antimicrobial resistance in 2019: a systematic analysis. Lancet 399:629-655.

3. Wang M, Earley M, Chen L, Hanson BM, Yu Y, Liu Z, Salcedo S, Cober E, Li L, Kanj SS, Gao H, Munita JM, Ordonez K, Weston G, Satlin MJ, Valderrama-Beltran SL, Marimuthu K, Stryjewski ME, Komarow L, Luterbach C, Marshall SH, Rudin SD, Manca C, Paterson DL, Reyes J, Villegas MV, Evans S, Hill C, Arias R, Baum K, Fries BC, Doi Y, Patel R, Kreiswirth BN, Bonomo RA, Chambers HF, Fowler VG, Jr., Arias CA, van Duin D, Multi-Drug Resistant Organism Network I. 2022. Clinical outcomes and bacterial characteristics of carbapenem-resistant Klebsiella pneumoniae complex among patients from different global regions (CRACKLE-2): a prospective, multicentre, cohort study. Lancet Infect Dis 22:401-412.

4. Xu L, Sun X, Ma X. 2017. Systematic review and meta-analysis of mortality of patients infected with carbapenem-resistant Klebsiella pneumoniae. Ann Clin Microbiol Antimicrob 16:18.

5. Agyeman AA, Bergen PJ, Rao GG, Nation RL, Landersdorfer CB. 2020. A systematic review and meta-analysis of treatment outcomes following antibiotic therapy among patients with carbapenem-resistant Klebsiella pneumoniae infections. Int J Antimicrob Agents 55:105833.

651 6. Martin RM, Cao J, Brisse S, Passet V, Wu W, Zhao L, Malani PN, Rao K, Bachman MA.
652 2016. Molecular Epidemiology of Colonizing and Infecting Isolates of Klebsiella
653 pneumoniae. mSphere 1.
654 7. Gorrie CL, Mirceta M, Wick RR, Edwards DJ, Thomson NR, Strugnell RA, Pratt NF,
655 Garlick JS, Watson KM, Pilcher DV, McGloughlin SA, Spelman DW, Jenney AWJ, Holt
656 KE. 2017. Gastrointestinal Carriage Is a Major Reservoir of Klebsiella pneumoniae
657 Infection in Intensive Care Patients. Clin Infect Dis 65:208-215.
658 8. Collingwood A, Blostein F, Seekatz AM, Wobus CE, Woods RJ, Foxman B, Bachman
659 MA. 2020. Epidemiological and Microbiome Associations Between Klebsiella
660 pneumoniae and Vancomycin-Resistant Enterococcus Colonization in Intensive Care
661 Unit Patients. Open Forum Infect Dis 7:ofaa012.
662 9. Selden R, Lee S, Wang WL, Bennett JV, Eickhoff TC. 1971. Nosocomial klebsiella
663 infections: intestinal colonization as a reservoir. Ann Intern Med 74:657-64.
664 10. Podschun R, Ullmann U. 1998. Klebsiella spp. as nosocomial pathogens: epidemiology,
665 taxonomy, typing methods, and pathogenicity factors. Clin Microbiol Rev 11:589-603.
666 11. Rao K, Patel A, Sun Y, Vornhagen J, Motyka J, Collingwood A, Teodorescu A, Baang
667 JH, Zhao L, Kaye KS, Bachman MA. 2021. Risk Factors for Klebsiella Infections among
668 Hospitalized Patients with Preexisting Colonization. mSphere
669 doi:10.1128/mSphere.00132-21:e0013221.
670 12. Conlan S, Kong HH, Segre JA. 2012. Species-level analysis of DNA sequence data
671 from the NIH Human Microbiome Project. PLoS One 7:e47075.
672 13. Martin RM, Cao J, Wu W, Zhao L, Manthei DM, Pirani A, Snitkin E, Malani PN, Rao K,
673 Bachman MA. 2018. Identification of Pathogenicity-Associated Loci in Klebsiella
674 pneumoniae from Hospitalized Patients. mSystems 3.

14. Vornhagen J, Bassis CM, Ramakrishnan S, Hein R, Mason S, Bergman Y, Sunshine N, Fan Y, Holmes CL, Timp W, Schatz MC, Young VB, Simner PJ, Bachman MA. 2021. A plasmid locus associated with Klebsiella clinical infections encodes a microbiome-dependent gut fitness factor. PLoS Pathog 17:e1009537.

15. Sorbara MT, Dubin K, Littmann ER, Moody TU, Fontana E, Seok R, Leiner IM, Taur Y, Peled JU, van den Brink MRM, Litvak Y, Baumler AJ, Chaubard JL, Pickard AJ, Cross JR, Pamer EG. 2019. Inhibiting antibiotic-resistant Enterobacteriaceae by microbiota-mediated intracellular acidification. J Exp Med 216:84-98.

16. Whelan KF, Colleran E, Taylor DE. 1995. Phage inhibition, colicin resistance, and tellurite resistance are encoded by a single cluster of genes on the IncHI2 plasmid R478. J Bacteriol 177:5016-27.

17. Marvin DS, Forrest ED. 1920. The Importance of Tellurium as a Health Hazard in Industry. A Preliminary Report. Public Health Reports (1896-1970) 35:939-954.

18. Chasteen TG, Fuentes DE, Tantalean JC, Vasquez CC. 2009. Tellurite: history, oxidative stress, and molecular mechanisms of resistance. FEMS Microbiol Rev 33:820-32.

19. Summers AO, Jacoby GA. 1977. Plasmid-determined resistance to tellurium compounds. J Bacteriol 129:276-81.

20. Morales EH, Pinto CA, Luraschi R, Munoz-Villagran CM, Cornejo FA, Simpkins SW, Nelson J, Arenas FA, Piotrowski JS, Myers CL, Mori H, Vasquez CC. 2017. Accumulation of heme biosynthetic intermediates contributes to the antibacterial action of the metalloid tellurite. Nat Commun 8:15320.

21. Perez JM, Calderon IL, Arenas FA, Fuentes DE, Pradenas GA, Fuentes EL, Sandoval JM, Castro ME, Elias AO, Vasquez CC. 2007. Bacterial toxicity of potassium tellurite: unveiling an ancient enigma. PLoS One 2:e211.

22. Turner RJ, Weiner JH, Taylor DE. 1995. The tellurite-resistance determinants tehAtehB and klaAklaBtelB have different biochemical requirements. Microbiology (Reading) 141 (Pt 12):3133-40.

23. Tremaroli V, Workentine ML, Weljie AM, Vogel HJ, Ceri H, Viti C, Tatti E, Zhang P, Hynes AP, Turner RJ, Zannoni D. 2009. Metabolomic investigation of the bacterial response to a metal challenge. Appl Environ Microbiol 75:719-28.

24. Anonymous. 2014. Isolation, identification and characterization of highly tellurite-resistant, tellurite-reducing bacteria from Antarctica. Polar Science 8:40 - 52.

25. Nedialkova LP, Denzler R, Koeppel MB, Diehl M, Ring D, Wille T, Gerlach RG, Stecher B. 2014. Inflammation fuels colicin Ib-dependent competition of Salmonella serovar Typhimurium and E. coli in enterobacterial blooms. PLoS Pathog 10:e1003844.

26. Chung LK, Raffatellu M. 2019. G.I. pros: Antimicrobial defense in the gastrointestinal tract. Semin Cell Dev Biol 88:129-137.

27. Lane MC, Alteri CJ, Smith SN, Mobley HL. 2007. Expression of flagella is coincident with uropathogenic Escherichia coli ascension to the upper urinary tract. Proc Natl Acad Sci U S A 104:16669-74.

28. Hilt EE, McKinley K, Pearce MM, Rosenfeld AB, Zilliox MJ, Mueller ER, Brubaker L, Gai X, Wolfe AJ, Schreckenberger PC. 2014. Urine is not sterile: use of enhanced urine culture techniques to detect resident bacterial flora in the adult female bladder. J Clin Microbiol 52:871-6.

29. Vornhagen J, Sun Y, Breen P, Forsyth V, Zhao L, Mobley HLT, Bachman MA. 2019. The Klebsiella pneumoniae citrate synthase gene, gltA, influences site specific fitness during infection. PLoS Pathog 15:e1008010.

30. Subashchandrabose S, Hazen TH, Brumbaugh AR, Himpsl SD, Smith SN, Ernst RD, Rasko DA, Mobley HL. 2014. Host-specific induction of Escherichia coli fitness genes during human urinary tract infection. Proc Natl Acad Sci U S A 111:18327-32.

31. McNally A, Alhashash F, Collins M, Alqasim A, Paszckiewicz K, Weston V, Diggle M. 2013. Genomic analysis of extra-intestinal pathogenic Escherichia coli urosepsis. Clin Microbiol Infect 19:E328-34.

32. Pajarillo EAB, Lee E, Kang DK. 2021. Trace metals and animal health: Interplay of the gut microbiota with iron, manganese, zinc, and copper. Anim Nutr 7:750-761.

33. Becker KW, Skaar EP. 2014. Metal limitation and toxicity at the interface between host and pathogen. FEMS Microbiol Rev 38:1235-49.

34. Palmer LD, Skaar EP. 2016. Transition Metals and Virulence in Bacteria. Annu Rev Genet 50:67-91.

35. Hryckowian AJ, Welch RA. 2013. RpoS contributes to phagocyte oxidase-mediated stress resistance during urinary tract infection by Escherichia coli CFT073. mBio 4:e00023-13.

36. Bessaiah H, Pokharel P, Loucif H, Kulbay M, Sasseville C, Habouria H, Houle S, Bernier J, Masse E, Van Grevenynghe J, Dozois CM. 2021. The RyfA small RNA regulates oxidative and osmotic stress responses and virulence in uropathogenic Escherichia coli. PLoS Pathog 17:e1009617.

37. Hennequin C, Forestier C. 2009. oxyR, a LysR-type regulator involved in Klebsiella pneumoniae mucosal and abiotic colonization. Infect Immun 77:5449-57.

38. Toptchieva A, Sisson G, Bryden LJ, Taylor DE, Hoffman PS. 2003. An inducible tellurite-resistance operon in Proteus mirabilis. Microbiology 149:1285-95.

39. Ni B, Zhang Y, Huang X, Yang R, Zhou D. 2014. Transcriptional regulation mechanism of ter operon by OxyR in Yersinia pestis. Curr Microbiol 69:42-6.

748 40. Wang Y, Branicky R, Noe A, Hekimi S. 2018. Superoxide dismutases: Dual roles in
749 controlling ROS damage and regulating ROS signaling. J Cell Biol 217:1915-1928.
750 41. Bachman MA, Breen P, Deornellas V, Mu Q, Zhao L, Wu W, Cavalcoli JD, Mobley HL.
751 2015. Genome-Wide Identification of Klebsiella pneumoniae Fitness Genes during Lung
752 Infection. MBio 6:e00775.
753 42. Najmuldeen H, Alghamdi R, Alghofaili F, Yesilkaya H. 2019. Functional assessment of
754 microbial superoxide dismutase isozymes suggests a differential role for each isozyme.
755 Free Radic Biol Med 134:215-228.
756 43. Anantharaman V, Iyer LM, Aravind L. 2012. Ter-dependent stress response systems:
757 novel pathways related to metal sensing, production of a nucleoside-like metabolite, and
758 DNA-processing. Mol Biosyst 8:3142-65.
759 44. Wang M, Chan EWC, Wan Y, Wong MH, Chen S. 2021. Active maintenance of proton
760 motive force mediates starvation-induced bacterial antibiotic tolerance in Escherichia
761 coli. Commun Biol 4:1068.
762 45. Verstraeten N, Knapen WJ, Kint CI, Liebens V, Van den Bergh B, Dewachter L, Michiels
763 JE, Fu Q, David CC, Fierro AC, Marchal K, Beirlant J, Versees W, Hofkens J, Jansen
764 M, Fauvart M, Michiels J. 2015. Obg and Membrane Depolarization Are Part of a
765 Microbial Bet-Hedging Strategy that Leads to Antibiotic Tolerance. Mol Cell 59:9-21.
766 46. Turkovicova L, Smidak R, Jung G, Turna J, Lubec G, Aradska J. 2016. Proteomic
767 analysis of the TerC interactome: Novel links to tellurite resistance and pathogenicity. J
768 Proteomics 136:167-73.
769 47. Balaban NQ, Helaine S, Lewis K, Ackermann M, Aldridge B, Andersson DI, Brynildsen
770 MP, Bumann D, Camilli A, Collins JJ, Dehio C, Fortune S, Ghigo JM, Hardt WD, Harms
771 A, Heinemann M, Hung DT, Jenal U, Levin BR, Michiels J, Storz G, Tan MW, Tenson T,

772 Van Melderen L, Zinkernagel A. 2019. Definitions and guidelines for research on
773 antibiotic persistence. Nat Rev Microbiol 17:441-448.
774 48. Westblade LF, Errington J, Dorr T. 2020. Antibiotic tolerance. PLoS Pathog
775 16:e1008892.
776 49. Lewis K. 2010. Persister cells. Annu Rev Microbiol 64:357-72.
777 50. Dorr T, Lewis K, Vulic M. 2009. SOS response induces persistence to fluoroquinolones
778 in Escherichia coli. PLoS Genet 5:e1000760.
779 51. Mao X, Auer DL, Buchalla W, Hiller KA, Maisch T, Hellwig E, Al-Ahmad A, Cieplik F.
780 2020. Cetylpyridinium Chloride: Mechanism of Action, Antimicrobial Efficacy in Biofilms,
781 and Potential Risks of Resistance. Antimicrob Agents Chemother 64.
782 52. Mike LA, Stark AJ, Forsyth VS, Vornhagen J, Smith SN, Bachman MA, Mobley HLT.
783 2021. A systematic analysis of hypermucoviscosity and capsule reveals distinct and
784 overlapping genes that impact Klebsiella pneumoniae fitness. PLoS Pathog
785 17:e1009376.
786 53. Miki T, Hardt WD. 2013. Outer membrane permeabilization is an essential step in the
787 killing of gram-negative bacteria by the lectin RegIIIbeta. PLoS One 8:e69901.
788 54. Rodrigues L, Ramos J, Couto I, Amaral L, Viveiros M. 2011. Ethidium bromide transport
789 across Mycobacterium smegmatis cell-wall: correlation with antibiotic resistance. BMC
790 Microbiol 11:35.
791 55. Sabnis A, Hagart KL, Klockner A, Becce M, Evans LE, Furniss RCD, Mavridou DA,
792 Murphy R, Stevens MM, Davies JC, Larrouy-Maumus GJ, Clarke TB, Edwards AM.
793 2021. Colistin kills bacteria by targeting lipopolysaccharide in the cytoplasmic
794 membrane. Elife 10.

795 56. Li J, Tang M, Liu Z, Xia F, Min C, Hu Y, Wang H, Zou M. 2022. Molecular and clinical
796 characterization of hypervirulent Klebsiella pneumoniae isolates from individuals with
797 urinary tract infections. Front Cell Infect Microbiol 12:925440.
798 57. Li J, Li Y, Tang M, Xia F, Min C, Hu Y, Wang H, Zhang J, Zou M. 2022. Distribution,
799 characterization, and antibiotic resistance of hypervirulent Klebsiella pneumoniae
800 isolates in a Chinese population with asymptomatic bacteriuria. BMC Microbiol 22:29.
801 58. Mataseje LF, Boyd DA, Mulvey MR, Longtin Y. 2019. Two Hypervirulent Klebsiella
802 pneumoniae Isolates Producing a bla KPC-2 Carbapenemase from a Canadian Patient.
803 Antimicrob Agents Chemother 63.
804 59. Karlsson M, Stanton RA, Ansari U, McAllister G, Chan MY, Sula E, Grass JE, Duffy N,
805 Anacker ML, Witwer ML, Rasheed JK, Elkins CA, Halpin AL. 2019. Identification of a
806 Carbapenemase-Producing Hypervirulent Klebsiella pneumoniae Isolate in the United
807 States. Antimicrob Agents Chemother 63.
808 60. Thorpe HA, Booton R, Kallonen T, Gibbon MJ, Couto N, Passet V, Lopez-Fernandez S,
809 Rodrigues C, Matthews L, Mitchell S, Reeve R, David S, Merla C, Corbella M, Ferrari C,
810 Comandatore F, Marone P, Brisse S, Sassera D, Corander J, Feil EJ. 2022. A large-
811 scale genomic snapshot of Klebsiella spp. isolates in Northern Italy reveals limited
812 transmission between clinical and non-clinical settings. Nat Microbiol
813 doi:10.1038/s41564-022-01263-0.
814 61. Lam MMC, Wick RR, Watts SC, Cerdeira LT, Wyres KL, Holt KE. 2021. A genomic
815 surveillance framework and genotyping tool for Klebsiella pneumoniae and its related
816 species complex. Nat Commun 12:4188.
817 62. Wyres KL, Lam MMC, Holt KE. 2020. Population genomics of Klebsiella pneumoniae.
818 Nat Rev Microbiol 18:344-359.

819 63. Muniz LR, Knosp C, Yeretssian G. 2012. Intestinal antimicrobial peptides during
820 homeostasis, infection, and disease. Front Immunol 3:310.
821 64. Zhao Y, Chen F, Wu W, Sun M, Bilotta AJ, Yao S, Xiao Y, Huang X, Eaves-Pyles TD,
822 Golovko G, Fofanov Y, D'Souza W, Zhao Q, Liu Z, Cong Y. 2018. GPR43 mediates
823 microbiota metabolite SCFA regulation of antimicrobial peptide expression in intestinal
824 epithelial cells via activation of mTOR and STAT3. Mucosal Immunol 11:752-762.
825 65. Yao X, Zhang C, Xing Y, Xue G, Zhang Q, Pan F, Wu G, Hu Y, Guo Q, Lu A, Zhang X,
826 Zhou R, Tian Z, Zeng B, Wei H, Strober W, Zhao L, Meng G. 2017. Remodelling of the
827 gut microbiota by hyperactive NLRP3 induces regulatory T cells to maintain
828 homeostasis. Nat Commun 8:1896.
829 66. Dorr T, Vulic M, Lewis K. 2010. Ciprofloxacin causes persister formation by inducing the
830 TisB toxin in Escherichia coli. PLoS Biol 8:e1000317.
831 67. Wong F, Stokes JM, Cervantes B, Penkov S, Friedrichs J, Renner LD, Collins JJ. 2021.
832 Cytoplasmic condensation induced by membrane damage is associated with antibiotic
833 lethality. Nat Commun 12:2321.
834 68. Castro ME, Molina RC, Diaz WA, Pradenas GA, Vasquez CC. 2009. Expression of
835 Aeromonas caviae ST pyruvate dehydrogenase complex components mediate tellurite
836 resistance in Escherichia coli. Biochem Biophys Res Commun 380:148-52.
837 69. Rai AK, Mitchell AM. 2020. Enterobacterial Common Antigen: Synthesis and Function of
838 an Enigmatic Molecule. mBio 11.
839 70. Lawlor MS, Hsu J, Rick PD, Miller VL. 2005. Identification of Klebsiella pneumoniae
840 virulence determinants using an intranasal infection model. Mol Microbiol 58:1054-73.
841 71. Botos I, Noinaj N, Buchanan SK. 2017. Insertion of proteins and lipopolysaccharide into
842 the bacterial outer membrane. Philos Trans R Soc Lond B Biol Sci 372.

843 72. Taylor PL, Sugiman-Marangos S, Zhang K, Valvano MA, Wright GD, Junop MS. 2010.
844 Structural and kinetic characterization of the LPS biosynthetic enzyme D-alpha,beta-D-
845 heptose-1,7-bisphosphate phosphatase (GmhB) from Escherichia coli. Biochemistry
846 49:1033-41.
847 73. Holmes CL, Smith SN, Gurczynski SJ, Severin GB, Unverdorben LV, Vornhagen J,
848 Mobley HLT, Bachman MA. 2022. The ADP-Heptose Biosynthesis Enzyme GmhB is a
849 Conserved Gram-Negative Bacteremia Fitness Factor. Infect Immun
850 doi:10.1128/iai.00224-22:e0022422.
851 74. Bontemps-Gallo S, Bohin JP, Lacroix JM. 2017. Osmoregulated Periplasmic Glucans.
852 EcoSal Plus 7.
853 75. Rosen DA, Pinkner JS, Walker JN, Elam JS, Jones JM, Hultgren SJ. 2008. Molecular
854 variations in Klebsiella pneumoniae and Escherichia coli FimH affect function and
855 pathogenesis in the urinary tract. Infect Immun 76:3346-56.
856 76. Hagberg L, Engberg I, Freter R, Lam J, Olling S, Svanborg Eden C. 1983. Ascending,
857 unobstructed urinary tract infection in mice caused by pyelonephritogenic Escherichia
858 coli of human origin. Infect Immun 40:273-83.
859 77. Frick-Cheng AE, Sintsova A, Smith SN, Krauthammer M, Eaton KA, Mobley HLT. 2020.
860 The Gene Expression Profile of Uropathogenic Escherichia coli in Women with
861 Uncomplicated Urinary Tract Infections Is Recapitulated in the Mouse Model. mBio 11.
862 78. Kanehisa M, Goto S. 2000. KEGG: kyoto encyclopedia of genes and genomes. Nucleic
863 Acids Res 28:27-30.
864 79. Kanehisa M, Sato Y, Kawashima M, Furumichi M, Tanabe M. 2016. KEGG as a
865 reference resource for gene and protein annotation. Nucleic Acids Res 44:D457-62.
866 80. UniProt C. 2021. UniProt: the universal protein knowledgebase in 2021. Nucleic Acids
867 Res 49:D480-D489.

868 81. Mi H, Muruganujan A, Ebert D, Huang X, Thomas PD. 2019. PANTHER version 14:
869 more genomes, a new PANTHER GO-slim and improvements in enrichment analysis
870 tools. Nucleic Acids Res 47:D419-D426.

871

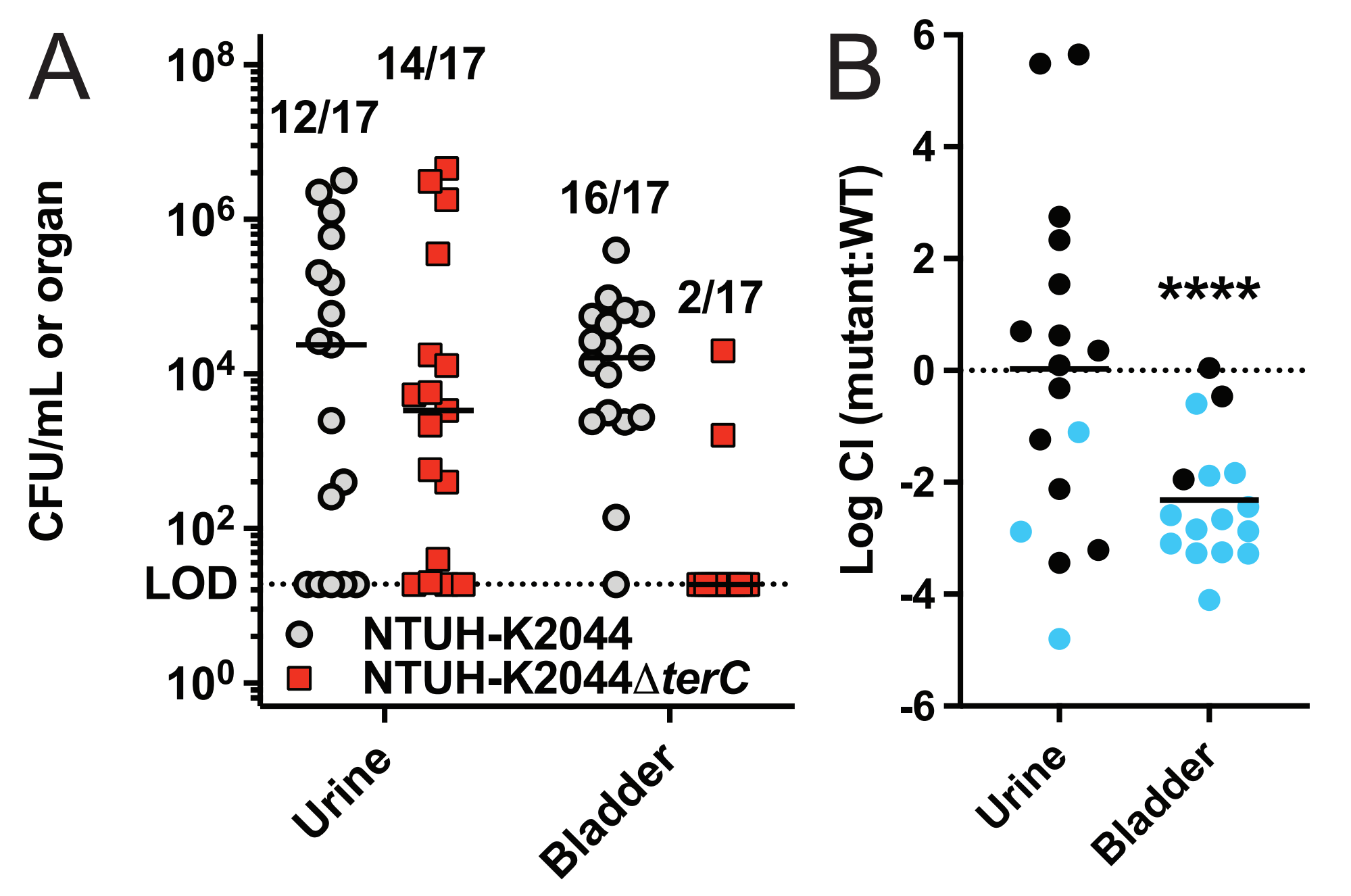
A
CFU/mL or organ
10^8
10^6
10^4
10^2
LOD
10^0
12/17
14/17
16/17
2/17
NTUH-K2044
NTUH-K2044ΔterC
Urine
Bladder
B
Log CI (mutant:WT)
6
4
2
0
-2
-4
-6
****
Urine
Bladder

A

K_2TeO_3

i

MIC (μM)

1024
512
256
128
64
32

**

ii

Fraction recovered

10
1
0.1
0.01
0.001
0.0001
0.00001
0.000001

iii

AUC

100
10
1

*

iv

Time (min)

1000
100
10
1

P = 0.1
*
*
*

v

Fraction recovered

10^{-2}
10^{-3}
10^{-4}
10^{-5}
10^{-6}
10^{-7}

P = 0.05
**
**

B

Ofloxacin

i

MIC (μg/mL)

1
0.5
0.25
0.125
0.0625

N.S.

ii

Fraction recovered

10
1
0.1
0.01
0.001
0.0001

iii

AUC

100
10
1
0.1

**

iv

Time (min)

1000
100
10
1
0.1

**
*
∞
∞

v

Fraction recovered

1
0.1
0.01
0.001
0.0001
0.00001

P = 0.94
*
*

C

PmB

i

MIC (μg/mL)

64
32
16
8

N.S.

ii

Fraction recovered

10
1
0.1
0.01
0.001

iii

AUC

100
10
1

*

iv

Time (min)

1000
100
10
1

P = 0.15
∞

v

Fraction recovered

1
0.1
0.01
0.001
0.0001
0.00001

P = 0.15
***
*

D

CPC

i

MIC (μM)

4
1
0.25
0.0625

N.S.

ii

Fraction recovered

10
1
0.1
0.01
0.001
0.0001
0.00001
0.000001

0
60
120
180
240

Time (min)

NTUH-K2044
NTUH-K2044Δ*terC*

iii

AUC

100
10
1
0.1

**

NTUH-K2044
terC

iv

Time (min)

1000
100
10
1
0.1

*
*
*
*

90
99
99.9
99.99

MDK

NTUH-K2044
NTUH-K2044Δ*terC*

v

Fraction recovered

10
1
0.1
0.01
0.001
0.0001
0.00001

*
**

NTUH-K2044pEmpty
NTUH-K2044Δ*terC*pEmpty
NTUH-K2044Δ*terC*pVector

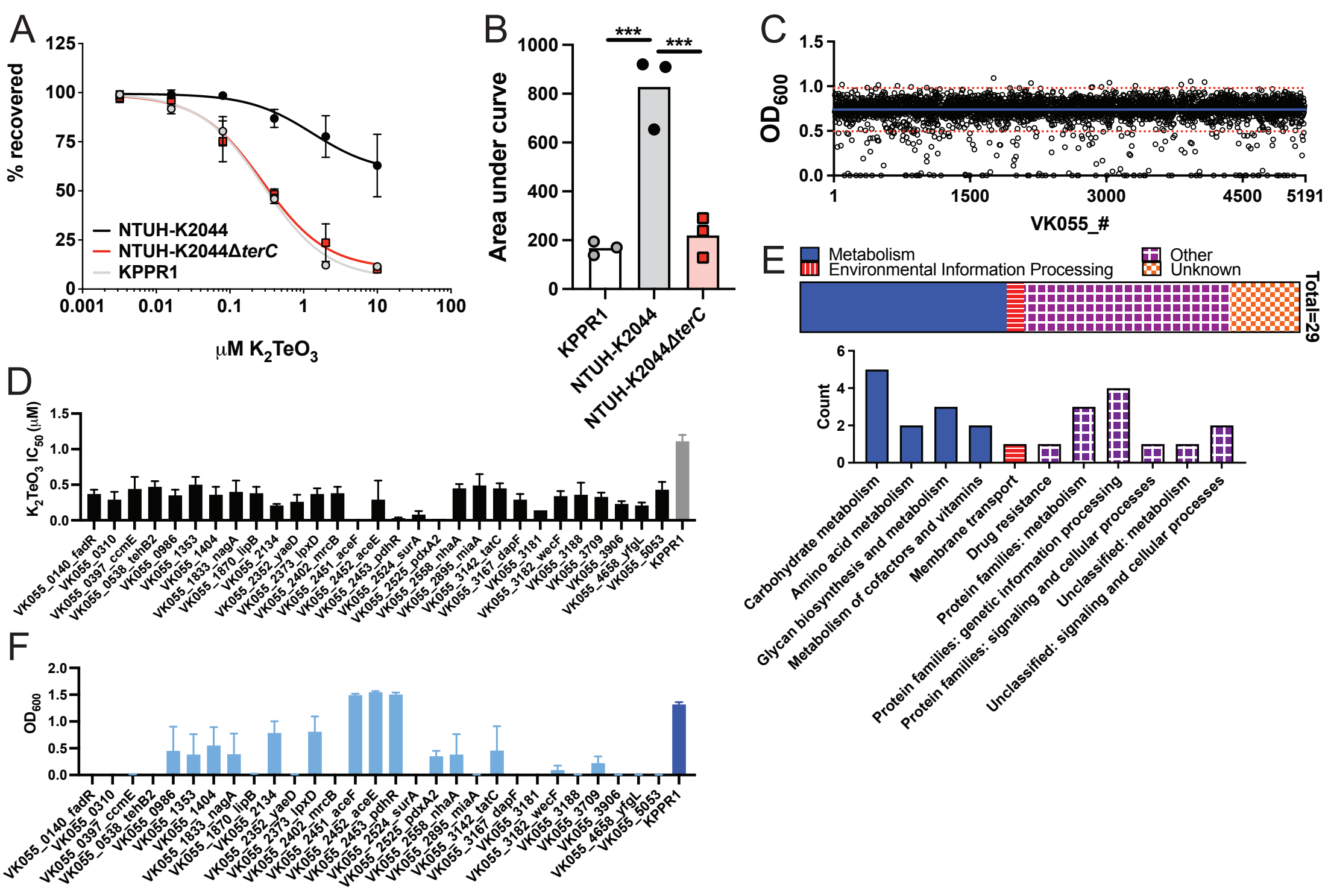
A
% recovered
125
100
75
50
25
0
0.001
0.01
0.1
1
10
100
μM K_2TeO_3
NTUH-K2044
NTUH-K2044ΔterC
KPPR1
B
Area under curve
1000
800
600
400
200
0
***
***
KPPR1
NTUH-K2044
NTUH-K2044ΔterC
C
OD_{600}
1.5
1.0
0.5
0.0
1
1500
3000
4500
5191
VK055_#
D
K_2TeO_3 IC_{50} (μM)
1.5
1.0
0.5
0.0
VK055_0140_fadR
VK055_0310
VK055_0397_ccmE
VK055_0538_tehB2
VK055_0986
VK055_1353
VK055_1404
VK055_1833_nagA
VK055_1870_lipB
VK055_2134
VK055_2352_yaeD
VK055_2373_lpxD
VK055_2402_mrcB
VK055_2451_aceF
VK055_2452_aceE
VK055_2453_pdhR
VK055_2524_surA
VK055_2525_pdxA2
VK055_2558_nhaA
VK055_2895_miaA
VK055_3142_tatC
VK055_3167_dapF
VK055_3181
VK055_3182_wecF
VK055_3188
VK055_3709
VK055_3906
VK055_4658_yfgL
VK055_5053
KPPR1
E
Metabolism
Environmental Information Processing
Other
Unknown
Total=29
Count
6
4
2
0
Carbohydrate metabolism
Amino acid metabolism
Glycan biosynthesis and metabolism
Metabolism of cofactors and vitamins
Membrane transport
Drug resistance
Protein families: metabolism
Protein families: genetic information processing
Protein families: signaling and cellular processes
Unclassified: metabolism
Unclassified: signaling and cellular processes
F
OD_{600}
2.0
1.5
1.0
0.5
0.0
VK055_0140_fadR
VK055_0310
VK055_0397_ccmE
VK055_0538_tehB2
VK055_0986
VK055_1353
VK055_1404
VK055_1833_nagA
VK055_1870_lipB
VK055_2134
VK055_2352_yaeD
VK055_2373_lpxD
VK055_2402_mrcB
VK055_2451_aceF
VK055_2452_aceE
VK055_2453_pdhR
VK055_2524_surA
VK055_2525_pdxA2
VK055_2558_nhaA
VK055_2895_miaA
VK055_3142_tatC
VK055_3167_dapF
VK055_3181
VK055_3182_wecF
VK055_3188
VK055_3709
VK055_3906
VK055_4658_yfgL
VK055_5053
KPPR1

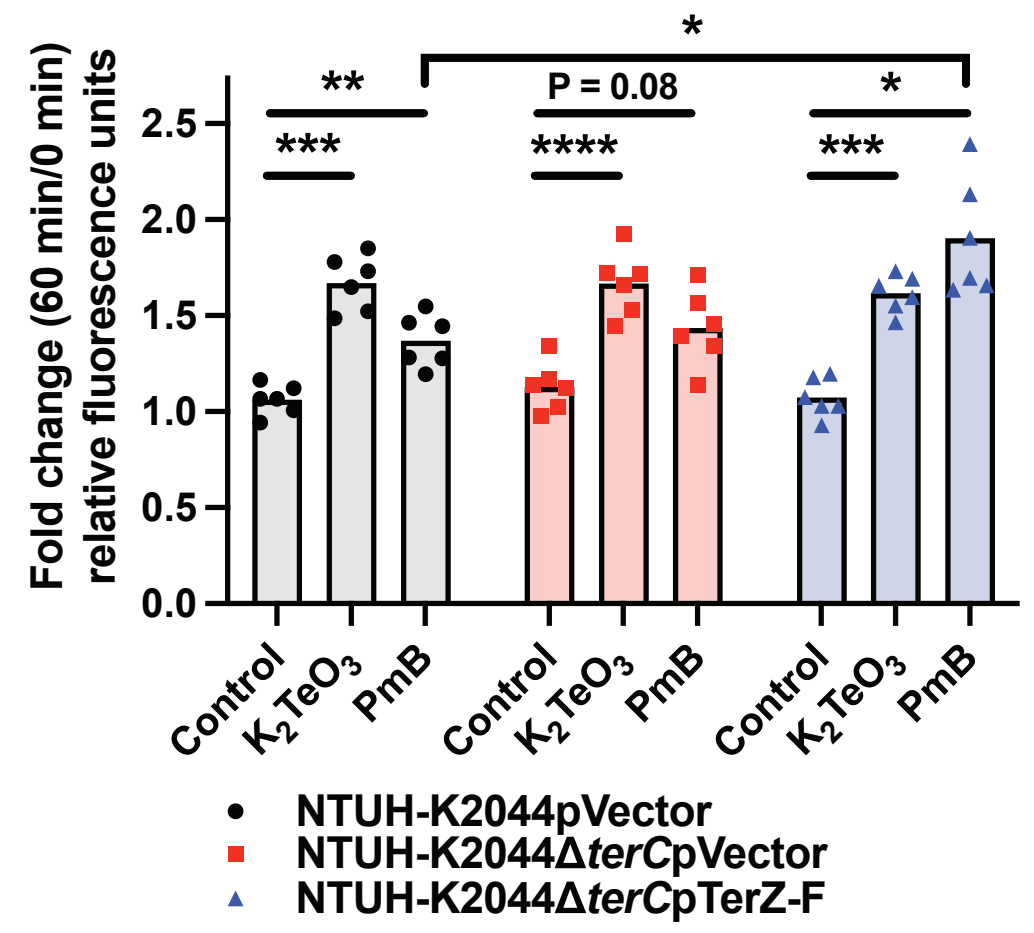
Fold change (60 min/0 min) relative fluorescence units
0.0
0.5
1.0
1.5
2.0
2.5
*
**
P = 0.08
*
***
****
***
Control
K2TeO3
PmB
Control
K2TeO3
PmB
Control
K2TeO3
PmB
NTUH-K2044pVector
NTUH-K2044ΔterCpVector
NTUH-K2044ΔterCpTerZ-F